IEEE Access
Multidisciplinary | Rapid Review | Open Access Journal

Received 2 March 2023, accepted 22 March 2023, date of publication 27 March 2023, date of current version 30 March 2023.

Digital Object Identifier 10.1109/ACCESS.2023.3262298

RESEARCH ARTICLE

Design and Analysis of a Compact Dual-Band Wearable Antenna for WBAN Applications

UMAR MUSA[1,3], (Student Member, IEEE), SHAHARIL MOHD SHAH[1], HUDA A. MAJID[1], (Member, IEEE), ISMAIL AHMAD MAHADI[2], (Student Member, IEEE), MOHAMAD KAMAL A. RAHIM[4], (Senior Member, IEEE), MUHAMMAD SANI YAHYA[5], (Graduate Student Member, IEEE), AND ZUHAIRIAH ZAINAL ABIDIN[1], (Senior Member, IEEE)

[1]Advanced Telecommunication Research Center (ATRC), Universiti Tun Hussein Onn Malaysia (UTHM), Batu Pahat, Johor 86400, Malaysia
[2]Faculty of Exact and Applied Science, University of N'Djamena, N'Djaména 1117, Chad
[3]Department of Electrical Engineering, Bayero University Kano, Kano 700006, Nigeria
[4]Advanced RF and Microwave Research Group, Faculty of Electrical Engineering, Universiti Teknologi Malaysia (UTM), Skudai, Johor 81310, Malaysia
[5]Department of Electrical and Electronics Engineering, Abubakar Tafawa Balewa University, Bauchi 740272, Nigeria

Corresponding authors: Shaharil Mohd Shah (shaharil@uthm.edu.my), Ismail Ahmad Mahadi (ismailaht@ieee.org), and Umar Musa (ge210004@student.uthm.edu.my)

This work was supported by the Ministry of Higher Education (MoHE), Malaysia, under FRGS Grant FRGS/1/2020/TK0/UTHM/02/44.

ABSTRACT The design and analysis of a compact dual-band wearable antenna for WBAN applications is presented. The antenna was prototyped on a semi-flexible Rogers Duroid RO3003™ with compact dimensions of $41 \times 44\ mm^2$ which corresponds to $0.33\ \lambda_0 \times 0.35\ \lambda_0$, where λ_0 is the free space wavelength at 2.4 GHz. The antenna is designed in the preliminary stage to resonate at 5.8 GHz. An inverted U-shaped slot is added to the patch to create one more resonant frequency at 2.4 GHz. To enhance the antenna's bandwidth and gain, two slots at the patch's bottom edge and a partial ground are added. The measured percentage of impedance bandwidth at 2.4 GHz and 5.8 GHz are 3.75% and 5.17%, respectively. The gain is measured to be 3.74 dBi and 5.13 dBi and the efficiency is 91.4% and 92.3%, respectively at the operating bands. The measured radiation patterns exhibit a bidirectional and directional radiation pattern in the *E*-plane at 2.4 GHz and 5.8 GHz bands, while omnidirectional radiation patterns are observed in the *H*-plane. At 2.4 GHz, the SAR limits are simulated to be 0.955 W/kg and 0.571 W/kg for 1 g and 10 g of human tissue, while at 5.8 GHz, the SAR limits are 0.478 W/kg and 0.127 W/kg, respectively. Therefore, the proposed antenna has met the FCC and ICNIRP standards. Bending conditions and on-body measurements of the proposed antenna indicate that the antenna's performance is unaffected. As a result, it is shown that the antenna possessed the ability to be utilized in WBAN applications.

INDEX TERMS Dual-band, patch antenna, WBAN applications, SAR, bending condition.

I. INTRODUCTION

Wireless Body Area Network (WBAN) has gained attention across various areas, including sports, security, health, and the military [1]. Based on the location of the signal nodes, WBAN communication modes are divided into three categories: on, off, and in-body modes [2], [3]. WBAN devices must meet the following requirement of low cost, low power consumption, higher bit rate, and the capacity to counteract changes in the human body [4]. The frequency assigned to WBAN is 400 MHz for medical implant communications networks, 2.4 GHz and 5.8 GHz for industrial, scientific, and medical (ISM) applications, and 3 GHz to 10 GHz are for ultra-wideband services (UWB) [5], [6]. Antennas for WBAN applications have drawn the attention of researchers since the human body actively uses these antennas. As a result, their performance may be impacted compared to antennas placed in free space due to the lossy and non-homogeneous coupling of the physical body [7], [8], [9]. Besides that, the effects of the antennas on human

The associate editor coordinating the review of this manuscript and approving it for publication was Giovanni Angiulli.

tissues must be considered, which can be evaluated based on its Specific Absorption Rate (SAR) limits which must abide by the Federal Communications Commission (FCC) and International Commission on Non-Ionizing Radiation Protection (ICNIRP) standards [10], [11], [12]. Microstrip patch antenna [8], [14], planar monopole [15], [16], planar inverted-F shaped [17], fractal [18], reconfigurable [19], and Substrate-Integrated Waveguide (SIW) [20] are some of the antennas proposed for WBAN applications. A patch antenna fabricated on Polydimethylsiloxane (PDMS) was presented in [21]. Similarly, Polyethylene Terephthalate (PET) was utilized in antenna design for WBAN applications [22]. Also, authors in [23] proposed a wearable antenna using SIW in which the antenna was attached to the substrate via a brass eyelet that connects to the ground plane via a hole. Authors in [24] proposed a paper-based star-shaped patch antenna for WBAN applications using L-stubs. In [25], a patch antenna on a silver-coated material was proposed for WBAN applications in which a half-mode substrate-integrated cavity model was used. However, these antenna designs have many limitations such as being larger in size, narrower bandwidth, lower gain, and high back radiation, as well as having constraints to be utilized in WBAN applications due to the rigid nature of the substrates used. Moreover, the semi-flexible characteristics of the Rogers Duroid RO3003^{TM} substrate material used for this work have addressed the rigidity and inflexibility issues associated with conventional antennas [26].

This work presents the design and analysis of a compact dual-band wearable antenna for WBAN applications. The antenna is designed and simulated to resonate at 5.8 GHz during the initial stage. To address the shortcomings of a single-band antenna, an inverted U-shaped slot is added to the patch to create one more resonant frequency at 2.4 GHz. Two slots at the patch's bottom edge and a partial ground are added to increase the antenna's bandwidth and gain. The antenna's performance under bending and SAR limits are also investigated to confirm that it is suitable for WBAN applications. Section II covers the proposed antenna's structure, parametric study, and the equivalent circuit model. Section III investigates the antenna's radiation characteristics. Section IV describes the bending investigation. The SAR analysis is presented in Section V. Section VI explores the antenna's performance close to the human body. Table 6 shows a comparison between the proposed antenna and some previous literature. Section VII includes the conclusion.

II. ANTENNA DESIGN

A. STRUCTURE AND DIMENSIONS

The design requirements for the proposed antenna are established first using the fundamental rectangular shape. The length and width of the patch are calculated using the transmission line model described in [27]. The CST MWS® software is used to evaluate changes in length, width, and gaps around the rectangular patch for this

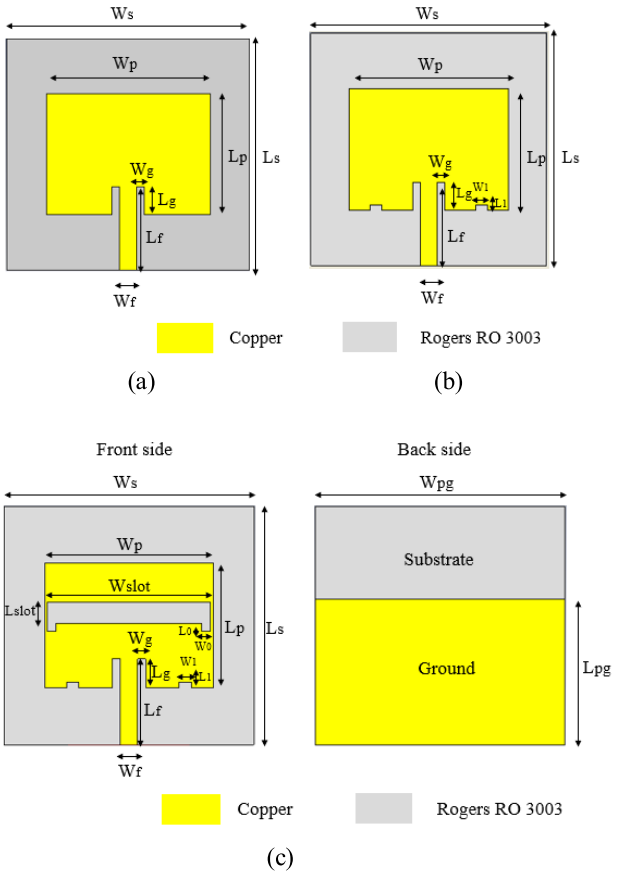

FIGURE 1. The proposed design's evolution (a) CPA (b) CPA with slots (c) proposed antenna.

structure, and the parameter values are optimized. According to a recent study in [28], adding slots to the radiating structure results in increased compactness and bandwidth, as well as generating another resonant frequencies.

At the preliminary design stage, the proposed antenna is designed and simulated using a Conventional Patch Antenna (CPA) to resonate at 5.8 GHz and is composed of a rectangular patch and inset microstrip feed line on a semi-flexible Rogers RO3003^{TM} substrate with a thickness, h of 1.52 mm, a dielectric constant, ε_r of 3, and a loss tangent, tan δ of 0.0013. At 5.8 GHz, the calculated length of the first design is 16.9 mm, and the optimized value is Lp = 21 mm. Furthermore, as shown in Fig. 1(a) and (b), the calculated width value at 5.8 GHz is 18.1 mm, while the optimized value is Wp = 29 mm. As seen in Fig. 1(c), an inverted U-shaped slot is then added to the patch to add a second resonant frequency at 2.4 GHz. Additionally, two slots and a partial ground are added to the patch's bottom edge to increase the antenna's bandwidth and gain. The optimized dimension of 41 × 44 mm^2 (0.33 λ_0 × 0.35 λ_0) was chosen. Table 1 summarizes the detailed dimensions of the proposed structure. Fig. 2 compares the simulated reflection coefficient (S_{11}) of the CPA with and without additional slots on the main radiating plane, demonstrating the achievement of dual-band

TABLE 1. Proposed antenna dimension.

Variables	Values (mm)	Variables	Values (mm)
Ls	41	W_f	2.98
Ws	44	Lf	15
Wp	29	Lg	5
Lp	21	Wg	2
Wpg	41	W_0	1.5
Lpg	25	L_0	1.4
W_{slot}	28	W_1	2.2
L_{slot}	3.7	L_1	1
h	1.52	T_p	0.035

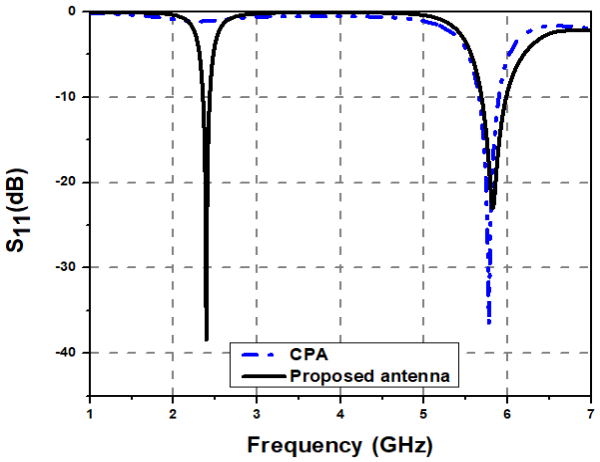

FIGURE 2. The simulated S_{11} with CPA and the proposed antenna.

TABLE 2. Proposed antenna performance.

Parameters	Proposed antenna		
	CPA	Proposed antenna	
Frequency (GHz)	5.8	2.4	5.8
Bandwidth (%)	4.9	3.8	5.2
Gain (dBi)	5.67	3.74	5.13
Efficiency (%)	92.9	91.4	92.3

frequencies. The lower frequency band is produced by the inverted U-shaped slot, which also reduced the dimensions of the antenna after optimization. The rectangular patch's two slots at the bottom do not affect the S_{11} of the antenna. The proposed antenna's simulation results are shown in Table 2 at various design phases.

B. PARAMETRIC STUDY

The effects of modifications on the antenna performance must be addressed and thus, a parametric study was performed to determine the optimal dimensions of the inset feed (Lg and

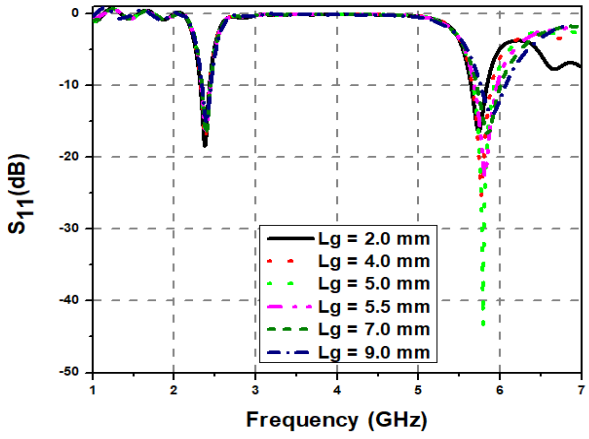

(a)

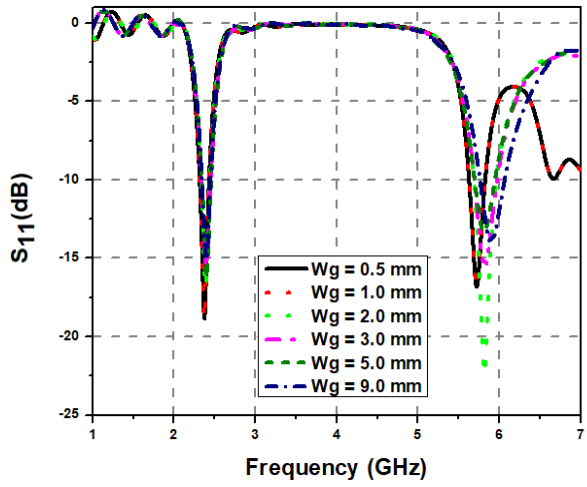

(b)

FIGURE 3. The simulated S_{11} with change to (a) Lg (b) Wg.

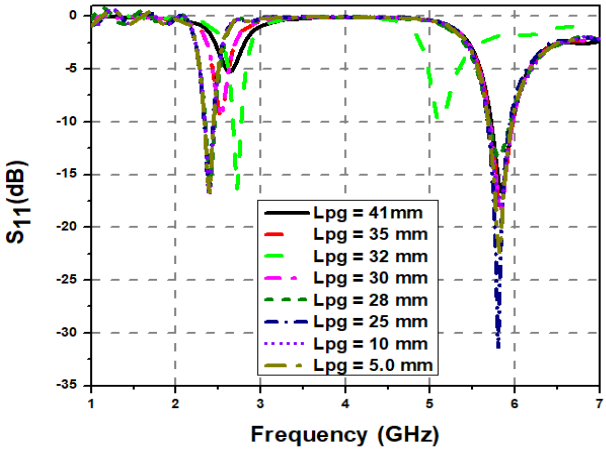

FIGURE 4. The simulated S_{11} with changing the ground plane's length.

Wg), as shown in Fig. 3(a) and (b). Moreover, a parametric study was also conducted on the length of the ground

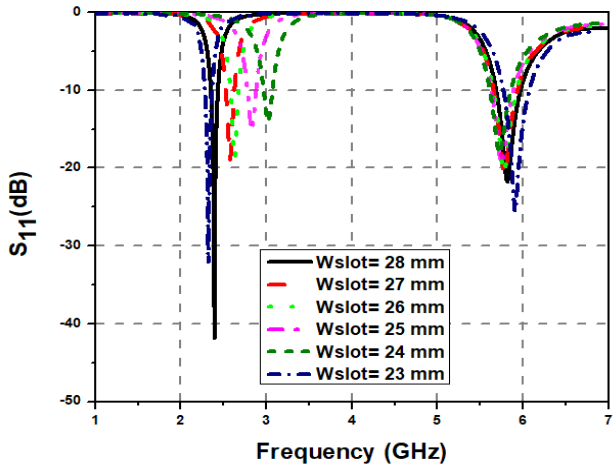

(a)

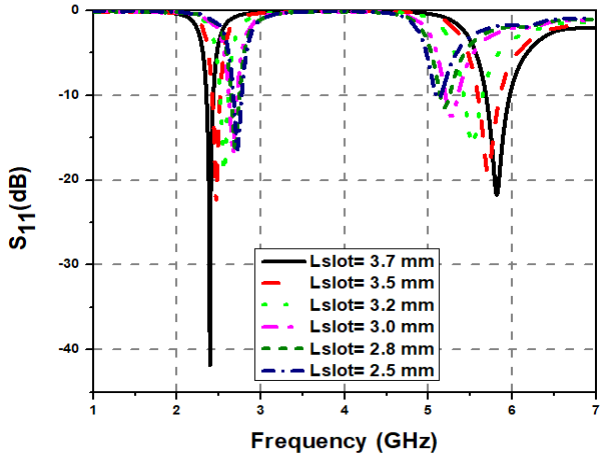

(b)

FIGURE 5. The simulated S_{11} with change to (a) Wslot (b) Lslot.

plane (L_{pg}) as seen in Fig. 4 with variations from 41 mm to 5.0 mm. From the parametric study, Lpg was found to be 25 mm, which also means that the antenna operates on a partial ground plane instead of a full ground plane. This also indicates that the ground plane does affect the antenna's performance. The inverted U-shaped slot width (W_{slot}) and length (L_{slot}), on the other hand, affect the lower and upper resonant frequencies of the antenna. A parametric study was also used to determine the optimum W_{slot} and L_{slot} as can be seen in Fig. 5. It can be seen from the figure that the resonant frequencies change with increasing width and length of the inverted U-shaped slot.

C. EQUIVALENT CIRCUIT

The equivalent circuit modelled with the Advanced Design System (ADS) software is shown in Fig. 6. The radiating patch is represented by the parallel lumped elements of

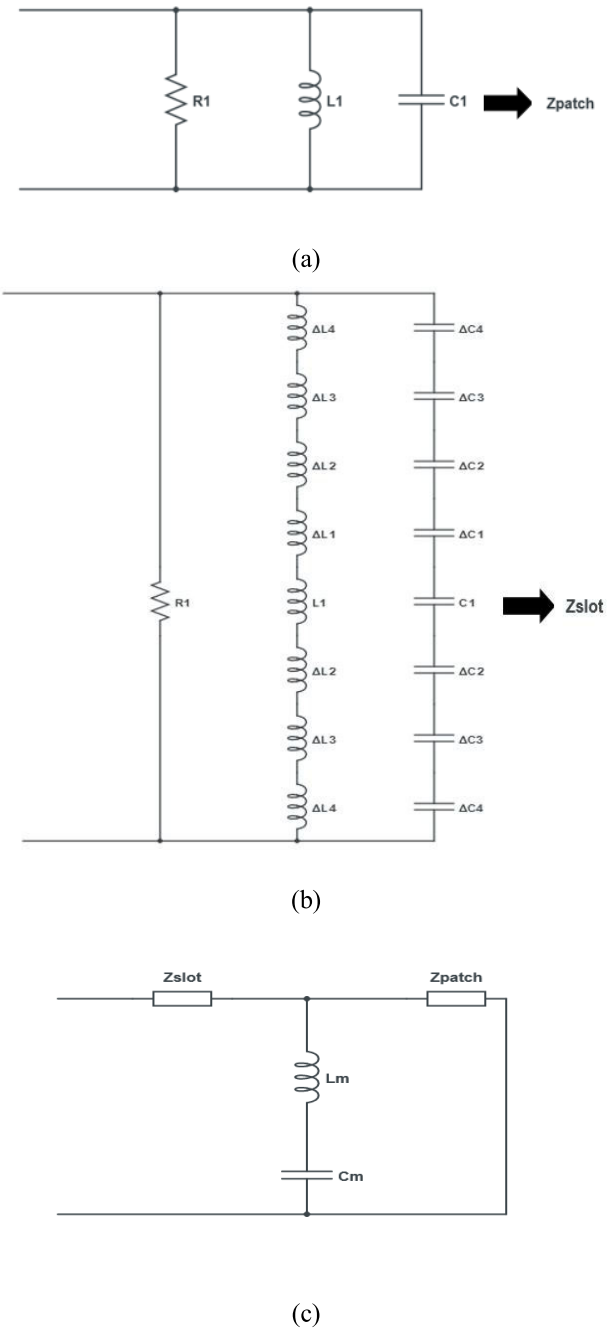

FIGURE 6. Equivalent circuit (a) Main radiating plane (b) Additional slots (c) Proposed antenna.

resistance (R1), inductance (L1), and capacitance (C1) as shown in Fig. 6(a) which allow the antenna to resonate at 5.8 GHz. R1, L1, and C1 values are calculated by using the equations in [29] and [30]. The inverted U-shaped slot and two additional slots are responsible for the 2.4 GHz band and can be expressed by a series of inductance and capacitance which are calculated by using the equations in [31] and [32]. The antenna's circuit is now modified as depicted in Fig. 6(b).

TABLE 3. Equivalent circuit component values.

Components	R1 (Ω)	L1 (nH)	C1 (pF)	ΔL1 (nH)	ΔL2 (nH)	ΔL3 (nH)	ΔL4 (nH)
Values	49.8	0.6	3.4	2.9	9.4	5.7	7.7
Components	ΔC1 (pF)	ΔC2 (pF)	ΔC3 (pF)	ΔC4 (pF)	L_m (nH)	C_m (pF)	
Values	2.3	1.6	5.5	0.9	0.6	2.9	

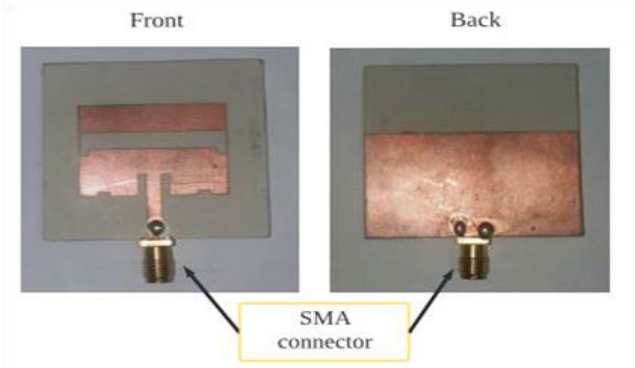

FIGURE 7. Proposed antenna prototype.

The radiating patch is made up of two surface current components: (i) the surface current that passes through the patch and (ii) a meandering surface current that passes around the inverted U-shaped slot, thus, increasing the surface current path [33]. The rectangular patch and additional slots equivalent circuits are combined via mutual inductance (Lm) and mutual capacitance (Cm) as shown in Fig. 6(c). The values of each element are listed in Table 3.

III. RESULTS AND ANALYSIS

To verify the design and simulations, the proposed antenna is fabricated as depicted in Fig. 7. The N5234B Keysight Vector Network Analyzer (VNA) and anechoic chamber are used for the measurement of the antenna's performance as depicted in Fig. 8. The S_{11} of the antenna is measured using the N5234B Keysight VNA, as shown in Fig. 8(a). In the anechoic chamber, as can be seen in Fig. 8(b), far field measurements which consist of radiation patterns and gain were carried out. The proposed antenna acts as a receiver, while a horn antenna moves in the azimuth and elevation planes as the transmitter.

A. REFLECTION COEFFICIENT

The S_{11} result's comparison of the proposed antenna is depicted in Fig. 9. The lower resonant frequency at 2.4 GHz has a -10 dB measured bandwidth of 3.8% from 2.358 GHz to 2.447 GHz, and the upper resonant frequency at 5.8 GHz is 5.2% from 5.675 GHz to 5.975 GHz. The figure demonstrates that the S_{11} results from the simulation, measurement, and equivalent circuit are all in satisfactory correlation.

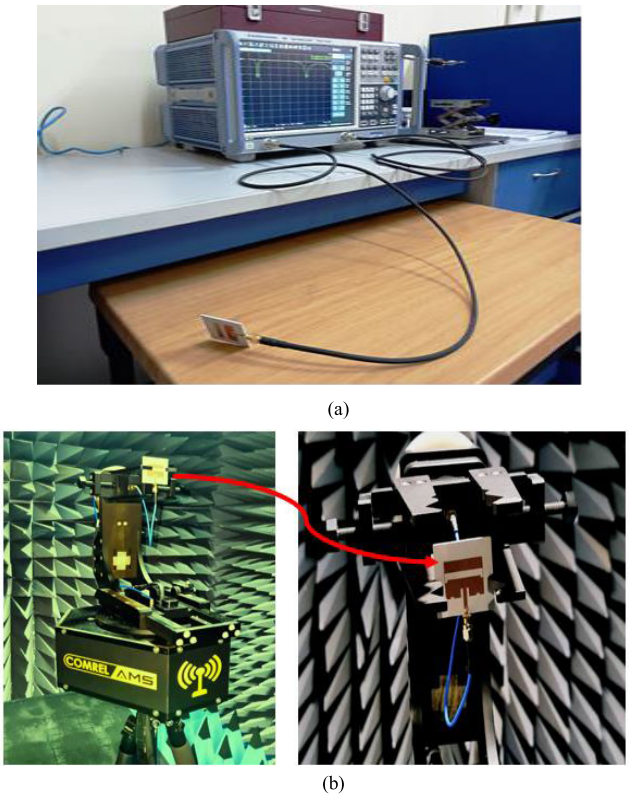

FIGURE 8. Antenna's measurement using: (a) N5234B Keysight VNA (b) Far-field measurements in the anechoic chamber.

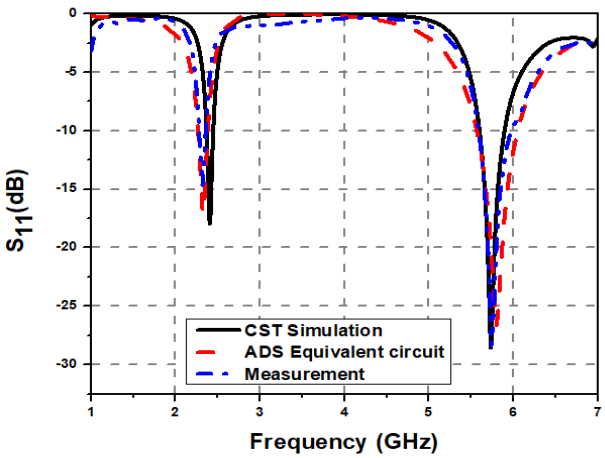

FIGURE 9. Comparison of the S_{11}.

B. CURRENT DISTRIBUTION

The antenna's current distribution is depicted in Fig. 10. The current distribution on the CPA is concentrated at the feed line and the edges of the patch, as seen in Fig. 10(a), demonstrating that it's responsible for the 5.8 GHz frequency. While the maximum current appears to be concentrated around the edges of the inverted U-shaped slot at 2.4 GHz with the additional slots, as shown in Fig. 10(b), the maximum current is most noticeable near the edges of the patch and the

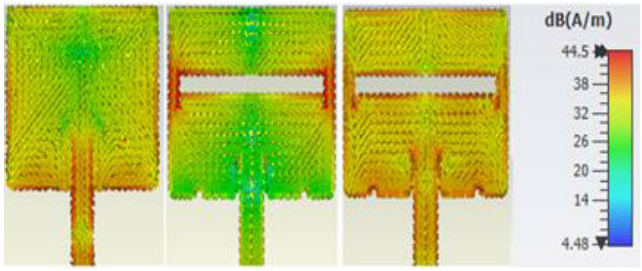

FIGURE 10. Current distributions on (a) CPA at 5.8 GHz (b) with inverted U-shaped slot at 2.4 GHz (c) with inverted U-shaped slot at 5.8 GHz.

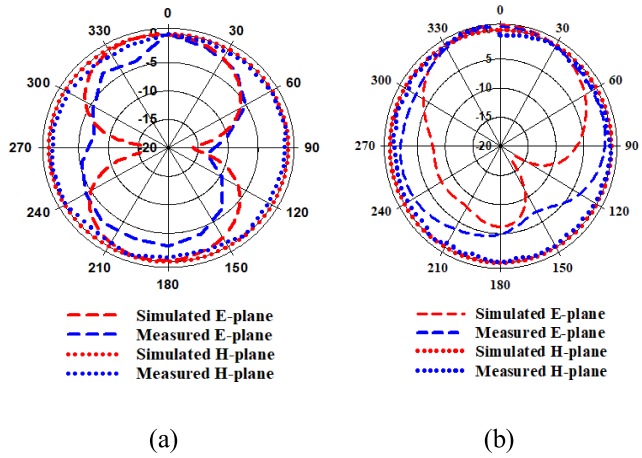

FIGURE 11. Radiation pattern *E*-plane and *H*-plane (a) 2.4 GHz (b) 5.8 GHz.

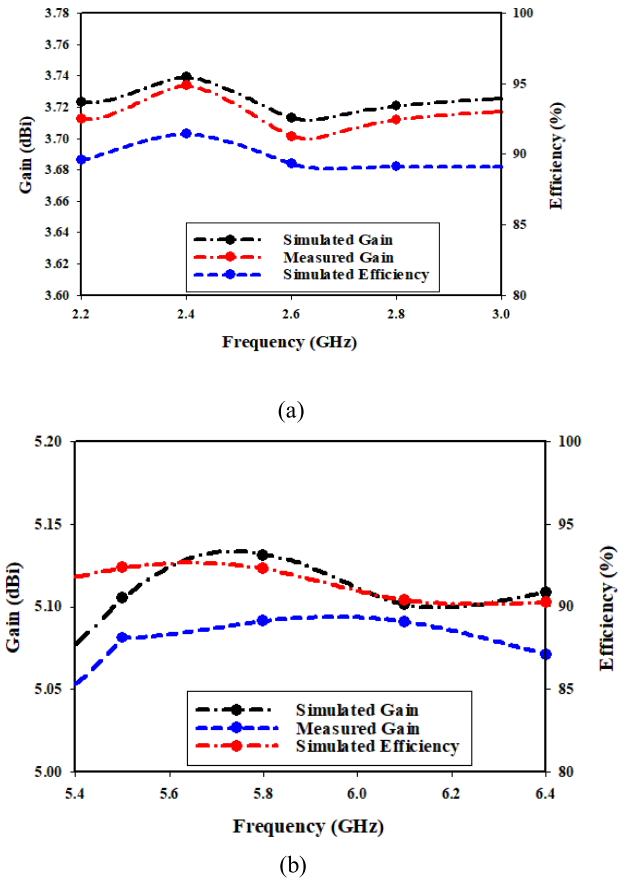

FIGURE 12. Gain vs efficiency at (a) 2.4 GHz (b) 5.8 GHz.

inverted U-shaped slot at 5.8 GHz, as shown in Fig. 10(c). The surface current distributions confirmed the antenna's preliminary design, which generated the 5.8 GHz through the CPA and 2.4 GHz by the rectangular patch's inverted U-shaped slot. These results align with the theoretical underpinnings presented in the earlier study [28], which state that the length of the current path on the patch has an impact on the frequency of operations.

C. RADIATION CHARACTERISTICS AND GAIN

The antenna's radiation characteristics are investigated using 2D and 3D radiation patterns at both the 2.4 GHz and 5.8 GHz resonant frequencies. Fig. 11(a) shows the 2D radiation patterns of the antenna at 2.4 GHz which are bidirectional in the *E*-plane and omnidirectional in the *H*-plane. At 5.8 GHz, the radiation patterns are directional in the *E*-plane and omnidirectional in the *H*-plane, as shown in Fig. 11(b). The proposed antenna can operate in both the 2.4 GHz and 5.8 GHz of the ISM bands with a gain of 3.74 dBi and 5.13 dBi and an efficiency of 91.4% and 92.3%, respectively, as shown in Fig. 12(a) and (b). The 3D far-field radiation patterns for the obtained frequency bands are shown in Fig. 13 for additional confirmation of the maximum gain attained by the proposed antenna.

IV. BENDING INVESTIGATION

Antennas might be bent when they are placed on human body. For this reason, the performance under bending conditions should be investigated for WBAN applications. The bending investigation is carried out along the y-axis and x-axis for both simulations and measurements, as illustrated in Fig. 14 and Fig. 15. The performance of the antenna under bending along the y-axis and x-axis is shown in Fig. 16 and Fig. 17, for diameters (d) of 50 mm, 80 mm, and 100 mm. The diameters chosen are based on the average size of human arms and legs. The simulated S_{11} are almost similar for both the y-axis and x-axis. However, in the y-axis, there is a small change in the S_{11} at the 5.8 GHz band when the diameter is decreased to 50 mm. The changes might be insignificant considering the small diameter. Styrofoam is used to measure the bending conditions for verification. The resonance frequencies for each Styrofoam diameter appear to have shifted slightly. However, the impact is thought to be minimal because the -10 dB bandwidth still accommodates the needed 2.4 GHz and 5.8 GHz frequency bands. The results from the simulation appear to be significantly more accurate than the measured result; this may be attributed to the use of Styrofoam, fabrication errors, and cable losses. Moreover, the radiation patterns across the three diameters from 50 mm to 100 mm

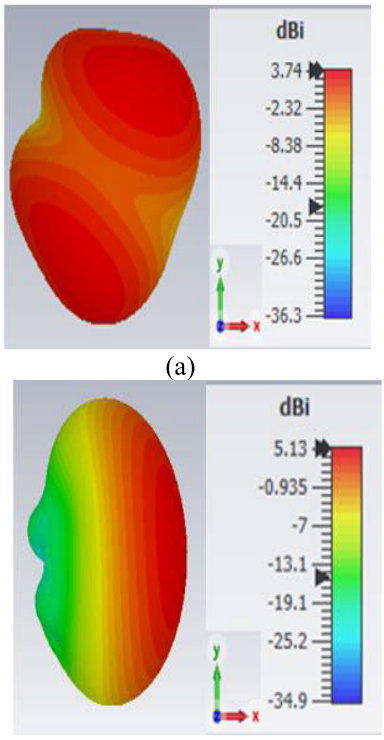

FIGURE 13. 3D radiation patterns at (a) 2.4 GHz (b) 5.8 GHz.

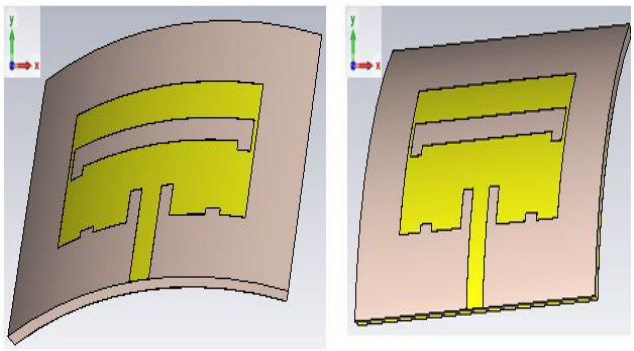

FIGURE 14. Proposed antenna bending (simulation) (a) y-axis (b) x-axis.

were investigated using simulation, and measurement was carried out with a 100 mm diameter as shown in Fig. 18 and Fig. 19. The radiation pattern across the diameters appears to be similar. There is a minor increase in back radiation when compared to the unbent scenario. This might happen as a result of minimal bending impacts on the materials. The gain achieved under bending ranges from 3.2 dBi and 5.2 dBi on the y-axis and x-axis for 2.4 GHz and 5.8 GHz, as shown in Fig 20(a) and (b).

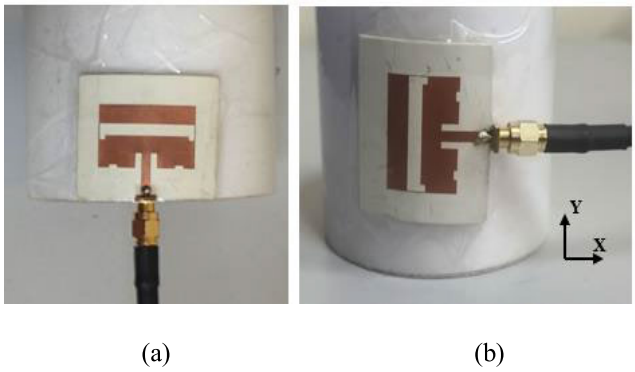

FIGURE 15. Proposed antenna bending (measurement) (a) y-axis (b) x-axis.

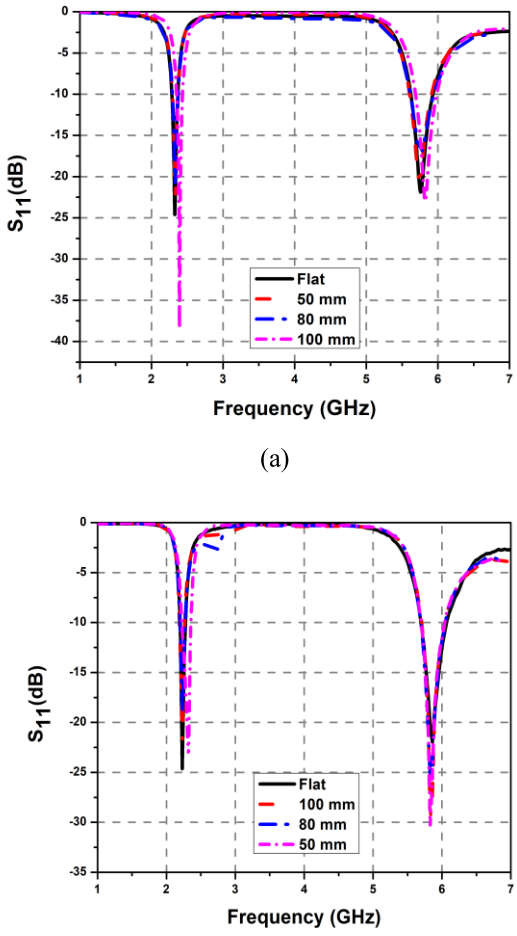

FIGURE 16. Design validation under bending along y-axis (a) simulation (b) measurement.

V. SAR ANALYSIS

Designing an antenna for WBAN applications necessitates measuring the SAR, as the antenna may be placed close to the human body. The SAR limits must not exceed 1.6 W/kg

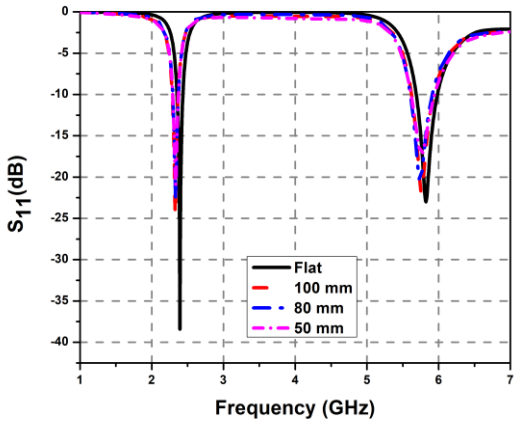

(a)

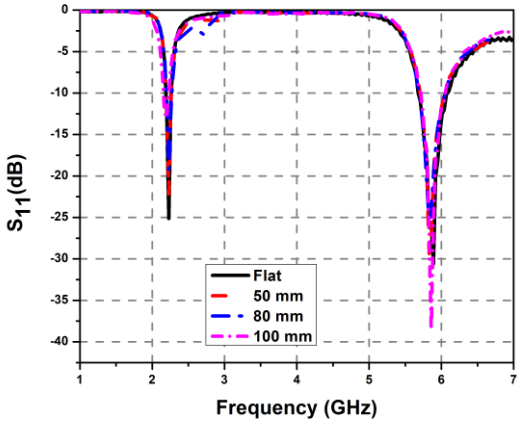

(b)

FIGURE 17. Design validation under bending along x-axis (a) simulation (b) measurement.

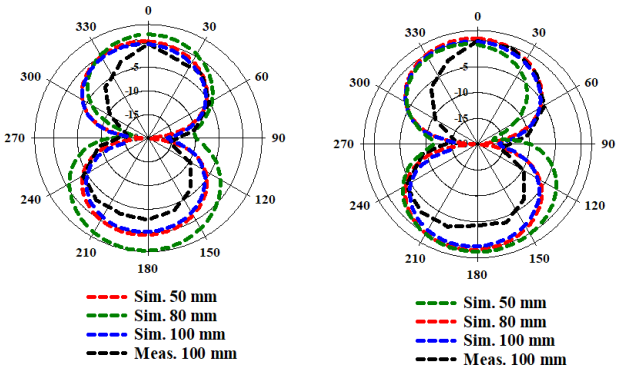

(a) (b)

FIGURE 18. Radiation pattern antenna bent at 2.4 GHz (a) y-axis (b) x-axis.

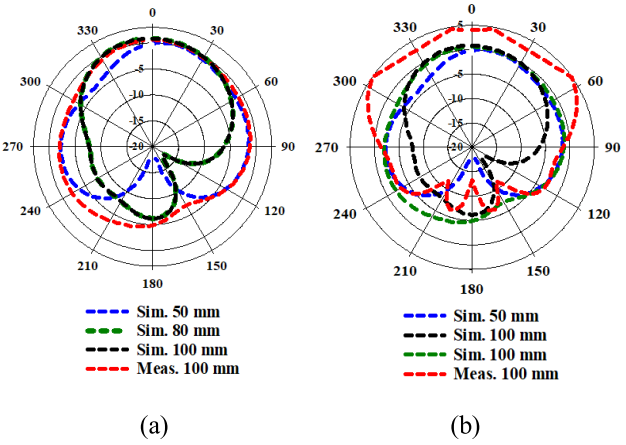

(a) (b)

FIGURE 19. Radiation pattern antenna bent at 5.8 GHz (a) y-axis (b) x-axis.

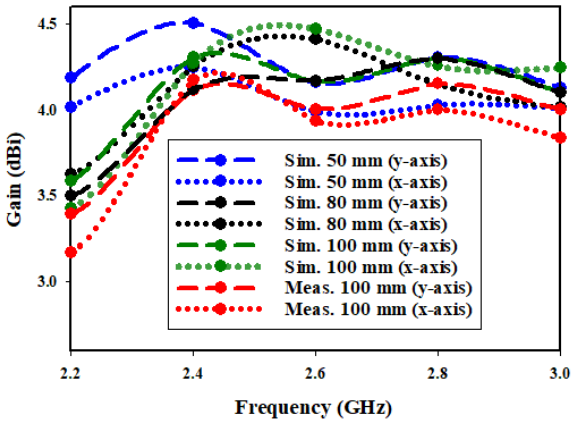

(a)

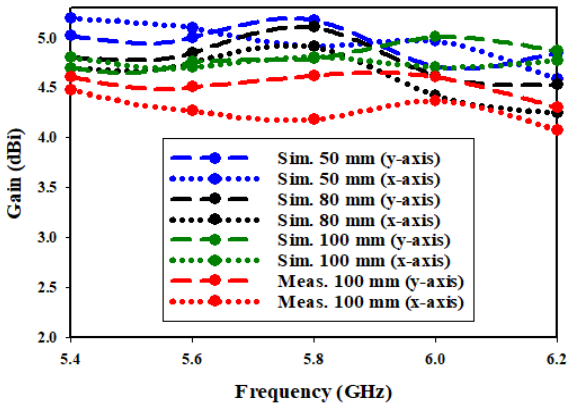

(b)

FIGURE 20. Measured gain for different bending conditions along the y-axis and x-axis (a) 2.4 GHz (b) 5.8 GHz.

per 1 g of tissue and 2 W/kg per 10 g of tissue as per FCC and ICNIRP standards [34], [35]. The SAR limits are calculated using the IEEE C95.1 standard in CST MWS® software.

In order to enhance the SAR limits, the input power was applied from 25 mW to 100 mW. The antenna was investigated by placing it at a distance of 2 mm, 4 mm, 6 mm, and 10 mm from the skin to account for a garment's

TABLE 4. The material parameter of layers of human body tissue models [7].

Layer	Skin	Fat	Muscle	Bone
Permittivity (F/m)	35.93	4.90	48.49	18.49
Density (kg/m^2)	1100	910	1040	1008
Conductivity (Ωm)	3.72	0.15	4.96	0.82
Thickness (mm)	2	5	20	13

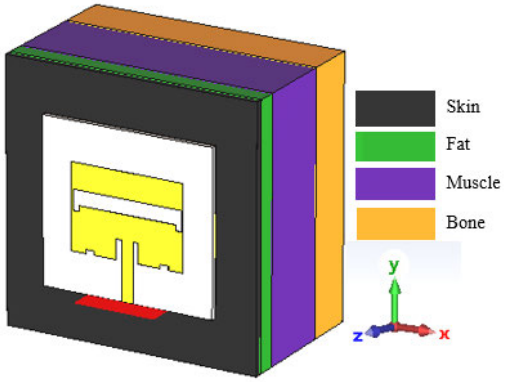

FIGURE 21. The simplified human body tissue model.

TABLE 5. Simulated SAR limits for 1 g and 10 g under varying incident power.

Incident Power (mW)	25		50		100		150	
Weight of human tissue	1g	10g	1g	10g	1g	10g	1g	10g
Freq. (GHz)	SAR limits (W/kg)							
2.4	0.46	0.27	0.75	0.49	0.96	0.57	1.12	0.89
5.8	0.23	0.14	0.39	0.35	0.48	0.13	0.79	0.51

thickness [36]. Table 4 lists the material parameter of layers of human body tissue model in the simulations and Fig. 21 shows the simplified human body tissue model made up of four layers: skin, fat, muscles, and bones. Their details and thickness were obtained from [7]. Table 5 shows the simulated SAR limits for 1 g and 10 g of human tissue at the resonant frequencies under varying input power.

Fig. 22 and Fig. 23 depict the antenna's SAR limits. According to Fig. 22(a) and (b), the SAR limits at 2.4 GHz for 1 g and 10 g of human tissue are 0.955 W/kg and 0.571 W/kg, respectively (with an input power of 100 mW). Furthermore, the SAR limits at 5.8 GHz are 0.127 W/kg and 0.478 W/kg for 1 g and 10 g of human tissue respectively as shown in Fig. 23(a) and (b). As a result, it is demonstrated that the SAR limits of the antenna in this work obey the FCC and ICNIRP standards.

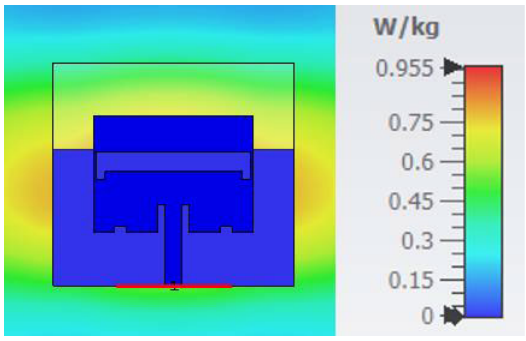

(a)

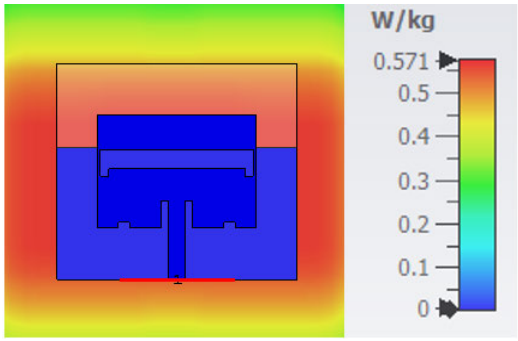

(b)

FIGURE 22. SAR limits (a) 1 g at 2.4 GHz (b) 10 g at 2.4 GHz (with an input power of 100 mW).

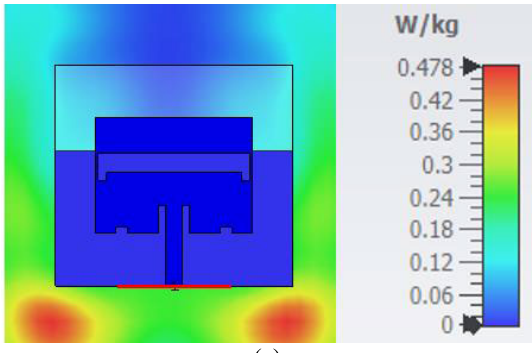

(a)

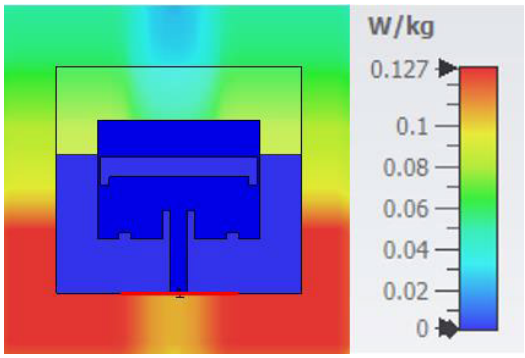

(b)

FIGURE 23. SAR limits (a) 1 g at 2.4 GHz (b) 10 g at 5.8 GHz (with an input power of 100 mW).

TABLE 6. Proposed antenna comparison with the antennas in previous work.

Ref	Dimensions (mm^2)	Frequency (GHz)	Substrate material	Bandwidth (%)	Gain (dBi)	SAR (W/kg)	Efficiency (%)	Substrate type
[37]	101.9 × 92.3	2.4/5.8	Felt	6.54/11.5	2.9/5.0	0.056/0.067	50/58	Flexible
[38]	19 × 12	2.4/5.8	Rogers	5.7/3.8	2.1/3.5	0.92/0.12	86/91	Semi-Flexible
[39]	50 × 50	2.4/5.8	FR-4	4.2/10.5	1.2/7.9	1.26/0.46	NA	Rigid
[40]	100 × 100	2.4/5.8	Felt	4.9/3.8	6.33/6.02	0.042/0.09	70.1/72.5	Flexible
[41]	50 × 50	2.4/5.8	Denim	NA	1.69/4.12	1.67/1.12	16/25	Flexible
[42]	40 × 30	2.4/3.5	FR-4	2.04/3.44	5.06/6.33	0.19/1.18	80/80	Rigid
[43]	30.5 × 62	2.4/5.8	Taconic TLY	3.47/2.58	1.51/6.44	NA	NA	Rigid
[44]	30 × 45	2.4/5.8	FR-4	4.9/2.8	3.09/0.64	NA	NA	Rigid
[45]	100 × 100	2.4/5.8	Felt	2.57/5.22	1.9/5.9	0.25/0.074	NA	Flexible
[46]	70 × 70	2.4/3.5	Felt	5.3/3.14	NA	NA	29/48	Flexible
[13]	30 × 38	2.4/5.8	Rogers	NA	NA	0.271/0.202	NA	Semi-Flexible
[47]	34 × 31	2.4/5.8	Kapton Polyimide	2.7/2.6	1.66/1.64	NA	91.6/91	Flexible
This work	**41 × 44**	**2.4/5.8**	**Rogers**	**3.8/5.2**	**3.74/5.13**	**0.57/0.13**	**91.4/92.3**	**Semi-Flexible**

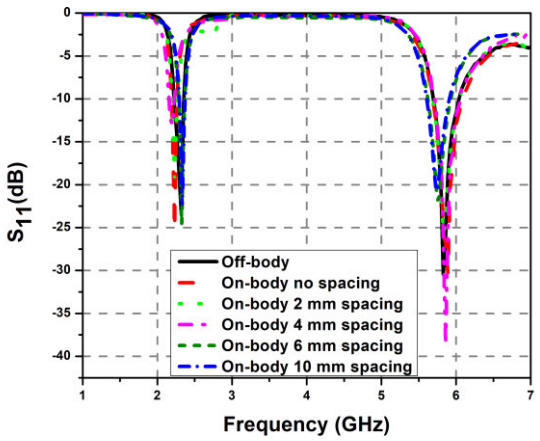

FIGURE 24. The simulated S_{11} results for varying thickness of a human garment between the proposed antenna and the human tissue model.

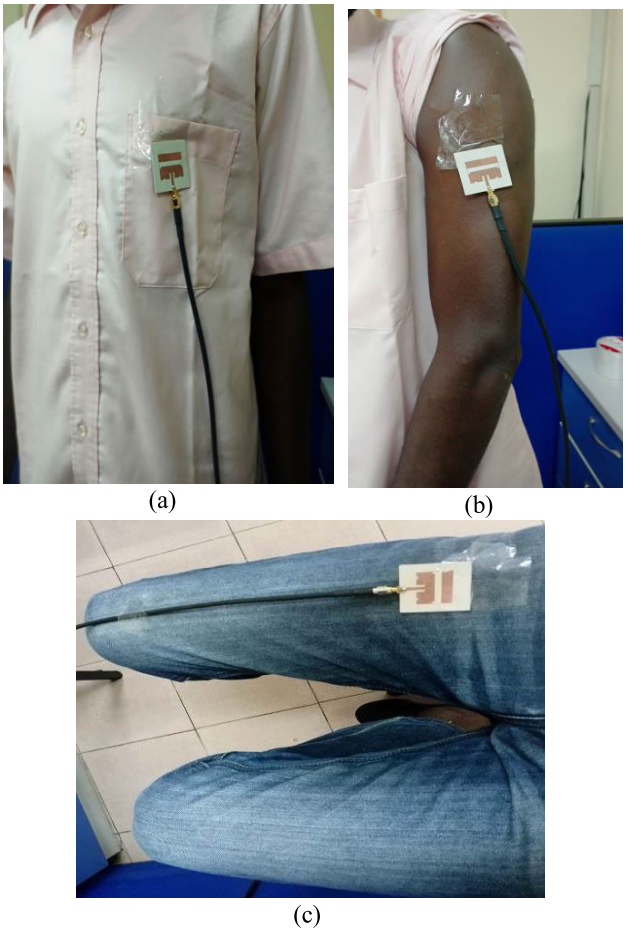

FIGURE 25. The proposed antenna is on (a) chest (b) arm (c) lap.

VI. ANTENNA'S PERFORMANCE NEAR HUMAN BODY

Since the antenna is intended to be used close to human body, the impact of the body on the overall performance was investigated. The simulated S_{11} for the antenna when it is placed directly on the skin and also on different garment's thicknesses from 2 mm to 10 mm is shown in Fig. 24. From the figure, the dual-band frequency was achieved throughout the simulations, even though the antenna is placed directly on the skin. Fig. 25 shows the antenna when it is placed on actual parts of a human body (chest, arm, and lap) to observe the dual-frequency variations. The measured S_{11}, on the other hand, can be viewed in Fig. 26. From the figure, there is a slight shift in the S_{11} when it is placed directly on the arm. This is due to human tissue having a high dielectric constant, which explains the changes in the lower resonant frequency [7]. Moreover, the radiation patterns when the antenna is placed on a human body tissue model were also

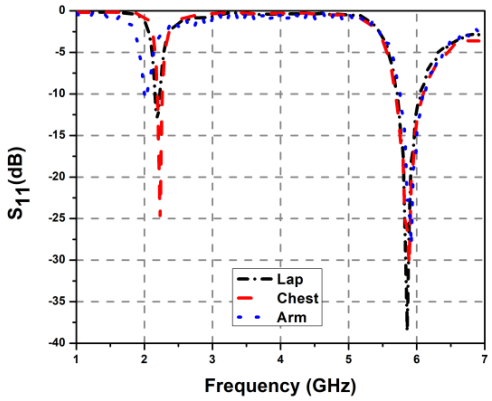

FIGURE 26. Performance of the proposed antenna on lap, chest, and arm.

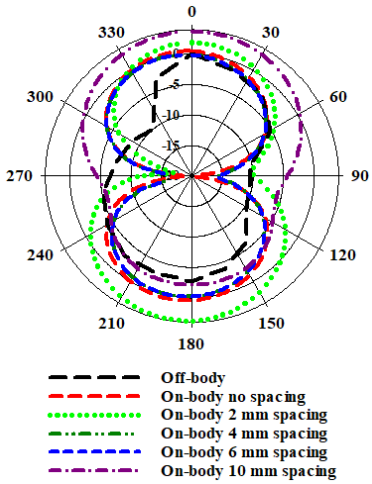

(a)

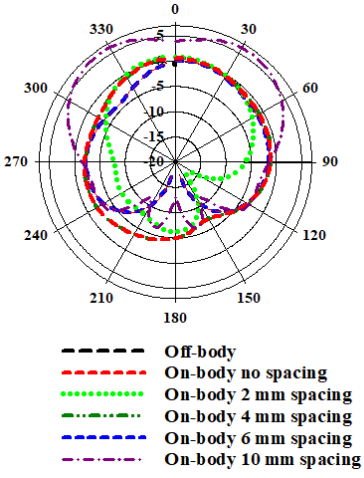

(b)

FIGURE 27. Radiation pattern loaded on human body phantom (a) 2.4 GHz (b) 5.8 GHz.

simulated (the antenna is placed directly on the skin and also on different garment's thicknesses from 2 mm to 10 mm),

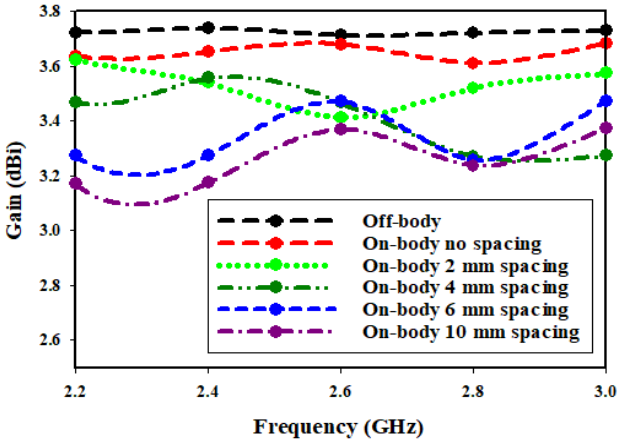

(a)

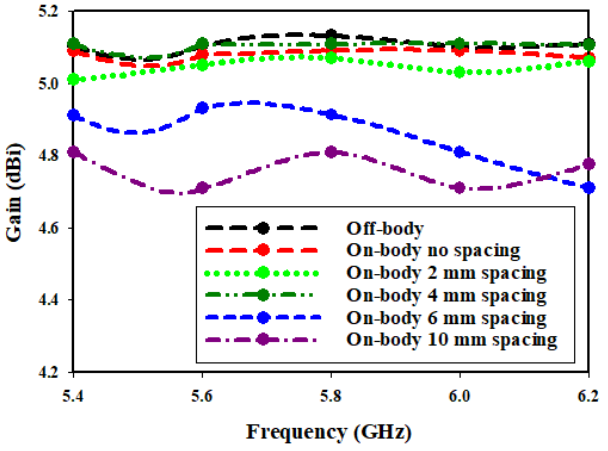

(b)

FIGURE 28. Gain on human phantom at (a) 2.4 GHz (b) 5.8 GHz.

as shown in Fig. 27. From the figure, the radiation patterns appear to be similar. The gain of the antenna, on the other hand, ranges from 3.0 dBi and 5.3 dBi on the x-axis and y-axis for both 2.4 GHz and 5.8 GHz, as shown in Fig. 28(a) and (b). A comparison of the proposed antenna in this work with the previous literature can be viewed in Table 6. From the table, the proposed antenna is considerably compact in dimensions as compared to the antennas presented in the previous work that utilize flexible, non-flexible, and semi-flexible substrates. Furthermore, the antenna's impedance bandwidth and gain are acceptable across the two operating bands.

VII. CONCLUSION

A compact dual-band wearable antenna for WBAN applications operating in the 2.4 GHz and 5.8 GHz ISM bands was designed and analyzed. The antenna structure consists of a CPA and an inverted U-shaped slot on it to generate dual-band frequencies. The inverted U-shaped slot is not only responsible for generating the lower frequency band but also for reducing the dimensions of the antenna upon optimization.

Two slots at the lower edge of the rectangular plane and partial ground plane are introduced to increase the bandwidth and gain of the antenna. The proposed antenna is fabricated on a semi-flexible Rogers Duroid RO3003^{TM} material with compact dimensions of 41 $\times$ 44 mm^2 which corresponds to 0.33 λ_0 $\times$ 0.35 λ_0. The measured percentage of impedance bandwidths at 2.4 GHz and 5.8 GHz are 3.75% and 5.17% respectively. The measured gain is 3.74 dBi and 5.13 dBi and the simulated radiation efficiency is 91.4% and 92.3% at the lower and upper resonant frequency, respectively. In terms of measured radiation patterns, bidirectional and directional radiation patterns are observed in the E-plane while omnidirectional radiation patterns are in the H-plane at the lower and upper resonant frequency, respectively. To investigate the potential of the dual-band antenna for WBAN applications, the SAR is simulated. The SAR limits at 2.4 GHz are 0.955 W/kg and 0.571 W/kg for 1 g and 10 g of human tissue, while at 5.8 GHz, the SAR limits are 0.478 W/kg and 0.127 W/kg, respectively. These values obey the FCC and ICNIRP standards. In addition, a bending investigation is also conducted on the antenna if it is to be worn on the human body such as on the lap, chest, and arm. It is shown from the results of the reflection coefficient that the performance of the antenna is not affected by bending. Therefore, it is safe to conclude that the proposed antenna is a good candidate for WBAN applications.

REFERENCES

[1] H. Yalduz, T. E. Tabaru, V. T. Kilic, and M. Turkmen, "Design and analysis of low profile and low SAR full-textile UWB wearable antenna with metamaterial for WBAN applications," *AEU Int. J. Electron. Commun.*, vol. 126, Nov. 2020, Art. no. 153465, doi: 10.1016/j.aeue.2020.153465.

[2] G.-P. Gao, Z.-H. Dou, Z.-Q. Yu, B.-K. Zhang, J.-H. Dong, and B. Hu, "Dual-mode patch antenna with capacitive coupling structure for on-/off-body applications," *IEEE Antennas Wireless Propag. Lett.*, vol. 21, no. 8, pp. 1512–1516, Aug. 2022, doi: 10.1109/LAWP.2022.3170555.

[3] N. Ziaei and A. Avokh, "Relay selection, clustering, and data aggregation routing in wireless body area networks," *Int. J. Commun. Syst.*, vol. 34, no. 10, p. e4837, Jul. 2021, doi: 10.1002/dac.4837.

[4] C. Mao, P. L. Werner, D. H. Werner, D. Vital, and S. Bhardwaj, "Dual-polarized armband embroidered textile antenna for on-/off-body wearable applications," in *Proc. IEEE Int. Symp. Antennas Propag. USNC-URSI Radio Sci. Meeting*, Jul. 2019, pp. 1555–1556, doi: 10.1109/APUSNCURSINRSM.2019.8889041.

[5] R. Sánchez-Montero, C. Camacho-Gómez, P.-L. López-Espí, and S. Salcedo-Sanz, "Optimal design of a planar textile antenna for industrial scientific medical (ISM) 2.4 GHz wireless body area networks (WBAN) with the CRO-SL algorithm," *Sensors*, vol. 18, no. 7, p. 1982, Jun. 2018, doi: 10.3390/s18071982.

[6] A. Yadav, V. K. Singh, A. K. Bhoi, G. Marques, B. Garcia-Zapirain, and I. de la Torre Díez, "Wireless body area networks: UWB wearable textile antenna for telemedicine and mobile health systems," *Micromachines*, vol. 11, no. 6, p. 558, May 2020, doi: 10.3390/mi11060558.

[7] U. Musa, S. M. Shah, H. A. Majid, Z. Z. Abidin, M. S. Yahya, S. Babani, and Z. Yunusa, "Recent advancement of wearable reconfigurable antenna technologies: A review," *IEEE Access*, vol. 10, pp. 121831–121863, 2022, doi: 10.1109/ACCESS.2022.3222782.

[8] A. Y. I. Ashyap, S. H. B. Dahlan, Z. Z. Abidin, S. K. A. Rahim, H. A. Majid, A. S. M. Alqadami, and M. El Atrash, "Fully fabric high impedance surface-enabled antenna for wearable medical applications," *IEEE Access*, vol. 9, pp. 6948–6960, 2021, doi: 10.1109/ACCESS.2021.3049491.

[9] S. Hussain, S. Hafeez, S. Ali, and N. Pirzada, "Design of wearable patch antenna for wireless body area networks," *Int. J. Adv. Comput. Sci. Appl.*, vol. 9, no. 9, 2018.

[10] H. S. Savcı and F. Kaburcuk, "FDTD-based SAR calculation of a wearable antenna for wireless body area network devices," *Int. J. Microw. Wireless Technol.*, vol. 14, pp. 1–7, Dec. 2022, doi: 10.1017/S1759078722001283.

[11] H. Savci, H. Sajjad, S. Khan, and F. Kaburcuk, "A compact multi-band antenna on textile for wearable body area network devices," *Balkan J. Electr. Comput. Eng.*, vol. 9, no. 3, pp. 255–260, Jul. 2021, doi: 10.17694/bajece.849699.

[12] R. Wu, J. Dong, and M. Wang, "Wearable polarization conversion metasurface MIMO antenna for biomedical applications in 5 GHz WBAN," *Biosensors*, vol. 13, no. 1, p. 73, Jan. 2023, doi: 10.3390/bios13010073.

[13] S. M. Shah, A. A. Rosman, M. A. Z. A. Rashid, Z. Z. Abidin, F. C. Seman, H. A. Majid, S. H. Dahlan, S. A. Hamzah, N. Katiran, A. Ponniran, F. Hassan, and F. Zubir, "A compact dual-band semi-flexible antenna at 2.45 GHz and 5.8 GHz for wearable applications," *Bull. Electr. Eng. Informat.*, vol. 10, no. 3, pp. 1739–1746, Jun. 2021, doi: 10.11591/eei.v10i3.2262.

[14] U. Mussa, M. K. A. Rahim, and M. A. Hamid, "Circular polarized textile antenna at 2.4 GHz," in *Proc. Int. Symp. Antennas Propag. (ISAP)*, Oct. 2016, pp. 964–965.

[15] S. Yan, L. A. Y. Poffelie, P. J. Soh, X. Zheng, and G. A. E. Vandenbosch, "On-body performance of wearable UWB textile antenna with full ground plane," in *Proc. 10th Eur. Conf. Antennas Propag. (EuCAP)*, Apr. 2016, pp. 1–4, doi: 10.1109/EuCAP.2016.7481477.

[16] S. Mohandoss, S. K. Palaniswamy, R. R. Thipparaju, M. Kanagasabai, B. R. B. Naga, and S. Kumar, "On the bending and time domain analysis of compact wideband flexible monopole antennas," *Int. J. Electron. Commun.*, vol. 101, pp. 168–181, Mar. 2019, doi: 10.1016/j.aeue.2019.01.015.

[17] G.-P. Gao, C. Yang, B. Hu, R.-F. Zhang, and S.-F. Wang, "A wearable PIFA with an all-textile metasurface for 5 GHz WBAN applications," *IEEE Antennas Wireless Propag. Lett.*, vol. 18, no. 2, pp. 288–292, Feb. 2019, doi: 10.1109/LAWP.2018.2889117.

[18] M. E. B. Jalil, M. K. A. Rahim, N. A. Samsuri, N. A. Murad, H. A. Majid, K. Kamardin, and M. A. Abdullah, "Fractal KOCH multiband textile antenna performance with bending, wet conditions and on the human body," *Prog. Electromagn. Res.*, vol. 140, pp. 633–652, 2013.

[19] S. N. Patil, P. V. Hungund, R. M. Vani, and H. V. M. Reddy, "Reconfigurable antenna for cognitive radio application using slot and parasitic patch," in *Proc. Int. Conf. Electr., Electron., Commun., Comput. Optim. Techn. (ICEECCOT)*, Dec. 2016, pp. 146–150, doi: 10.1109/ICEECCOT.2016.7955204.

[20] Y. Hong, J. Tak, and J. Choi, "An all-textile SIW cavity-backed circular ring-slot antenna for WBAN applications," *IEEE Antennas Wireless Propag. Lett.*, vol. 15, pp. 1995–1999, Apr. 2016, doi: 10.1109/LAWP.2016.2549578.

[21] J.-H. So, J. Thelen, A. Qusba, G. J. Hayes, G. Lazzi, and M. D. Dickey, "Reversibly deformable and mechanically tunable fluidic antennas," *Adv. Funct. Mater.*, vol. 19, no. 22, pp. 3632–3637, 2009, doi: 10.1002/adfm.200900604.

[22] S. G. Kirtania, A. W. Elger, M. R. Hasan, A. Wisniewska, K. Sekhar, T. Karacolak, and P. K. Sekhar, "Flexible antennas: A review," *Micromachines*, vol. 11, no. 9, p. 847, Sep. 2020, doi: 10.3390/mi11090847.

[23] R. Moro, S. Agneessens, H. Rogier, A. Dierck, and M. Bozzi, "Textile microwave components in substrate integrated waveguide technology," *IEEE Trans. Microw. Theory Techn.*, vol. 63, no. 2, pp. 422–432, Feb. 2015, doi: 10.1109/TMTT.2014.2387272.

[24] W. N. Marzudi, Z. Z. Abidin, S. H. Dahlan, K. N. Ramli, and M. R. Kamarudin, "Performance of star patch antenna on a paper substrate material," *ARPN J. Eng. Appl. Sci.*, vol. 10, pp. 8606–8612, Oct. 2015.

[25] T. Kaufmann and C. Fumeaux, "Wearable textile half-mode substrate-integrated cavity antenna using embroidered vias," *IEEE Antennas Wireless Propag. Lett.*, vol. 12, pp. 805–808, 2013, doi: 10.1109/LAWP.2013.2270939.

[26] C. A. Ed Balanis, *Modern Antenna Handbook*. Hoboken, NJ, USA: Wiley, 2011.

[27] F. Hirtenfelder, "Effective antenna simulations using CST MICROWAVE STUDIO®," in *Proc. 2nd Int. ITG Conf. Antennas*, 2007, p. 239, doi: 10.1109/INICA.2007.4353972.

[28] U. Musa, S. Babani, Z. Yunusa, and A. S. Ali, "Bandwidth enhancement of microstrip patch antenna using slits for 5G mobile communication networks," in *Proc. Int. Symp. Antennas Propag. (ISAP)*, Jan. 2021, pp. 559–560, doi: 10.23919/ISAP47053.2021.9391151.

[29] A. Roy, S. Bhunia, D. C. Sarkar, P. P. Sarkar, and S. K. Chowdhury, "Compact multi frequency strip loaded microstrip patch antenna with spurlines," *Int. J. Microw. Wireless Technol.*, vol. 9, no. 5, pp. 1111–1121, Jun. 2017, doi: 10.1017/S1759078716001136.
[30] M. Aneesh, J. A. Ansari, and A. Singh, "Analysis of S-shape microstrip patch antenna for Bluetooth application," *Int. J. Sci. Res. Publications*, vol. 3, no. 11, pp. 1–4, 2013.
[31] V. K. Pandey and B. Vishvakarma, "Theoretical analysis of linear array antenna of stacked patches," *Indian J. Radio Space Phys.*, vol. 34, pp. 125–130, Apr. 2005.
[32] M. K. Meshram and B. R. Vishvakarma, "Gap-coupled microstrip array antenna for wide-band operation," *Int. J. Electron.*, vol. 88, no. 11, pp. 1161–1175, Nov. 2001, doi: 10.1080/00207210110071288.
[33] A. A. Deshmukh, A. Mhatre, C. Kudoo, and S. Pawar, "E-shape microstrip antenna backed by pairs of slots cut ground plane for wideband response," *Proc. Comput. Sci.*, vol. 143, pp. 101–107, Jan. 2018, doi: 10.1016/j.procs.2018.10.357.
[34] International Commission on Non-Ionizing Radiation Protection, "Guidelines for limiting exposure to time-varying electric, magnetic, and electromagnetic fields (up to 300 GHz)," *Health Phys.*, vol. 74, no. 4, pp. 494–522, 1998.
[35] *IEEE Standard for Safety Levels With Respect to Human Exposure to Radio Frequency Electromagnetic Fields, 3 kHz to 300 GHz*, IEEE Standard C95.1 Edition-1999, Apr. 1999, pp. 1–83, doi: 10.1109/IEEESTD.1999.89423.
[36] S. Rajebi, C. Ghobadi, J. Nourinia, and E. Mostafapour, "SAR enhancement of slot microstrip antenna by using silicon layer in hyperthermia applications," *Wireless Pers. Commun.*, vol. 111, no. 3, pp. 1761–1774, Apr. 2020, doi: 10.1007/s11277-019-06955-1.
[37] S. Yan, P. J. Soh, and G. A. E. Vandenbosch, "Dual-band textile MIMO antenna based on substrate-integrated waveguide (SIW) technology," *IEEE Trans. Antennas Propag.*, vol. 63, no. 11, pp. 4640–4647, Nov. 2015, doi: 10.1109/TAP.2015.2477094.
[38] T. T. Le and T.-Y. Yun, "Miniaturization of a dual-band wearable antenna for WBAN applications," *IEEE Antennas Wireless Propag. Lett.*, vol. 19, no. 8, pp. 1452–1456, Aug. 2020, doi: 10.1109/LAWP.2020.3005658.
[39] C. Zhao and W. Geyi, "Design of a dual band dual mode antenna for on/off body communications," *Microw. Opt. Technol. Lett.*, vol. 62, no. 1, pp. 514–520, Jan. 2020, doi: 10.1002/mop.32085.
[40] L. Zhou, S. Fang, and X. Jia, "Dual-band and dual-polarised circular patch textile antenna for on/off-body WBAN applications," *IET Microw., Antennas Propag.*, vol. 14, no. 7, pp. 643–648, Jun. 2020, doi: 10.1049/iet-map.2019.1073.
[41] S. Bhattacharjee, S. Maity, S. R. B. Chaudhuri, and M. Mitra, "A compact dual-band dual-polarized omnidirectional antenna for on-body applications," *IEEE Trans. Antennas Propag.*, vol. 67, no. 8, pp. 5044–5053, Aug. 2014, doi: 10.1109/TAP.2019.2891633.
[42] S. Ahmad, A. Ghaffar, N. Hussain, and N. Kim, "Compact dual-band antenna with paired L-shape slots for on- and off-body wireless communication," *Sensors*, vol. 21, no. 23, p. 7953, 2021, doi: 10.3390/s21237953.
[43] Y. Hong, J. Tak, and J. Choi, "Dual-band dual-mode patch antenna for on–on–off WBAN applications," *Electron. Lett.*, vol. 50, no. 25, pp. 1895–1896, Dec. 2014, doi: 10.1049/el.2014.2551.
[44] J. Tak, S. Woo, J. Kwon, and J. Choi, "Dual-band dual-mode patch antenna for on-/off-body WBAN communications," *IEEE Antennas Wireless Propag. Lett.*, vol. 15, pp. 348–351, 2016, doi: 10.1109/LAWP.2015.2444881.
[45] L. Zhou, S.-J. Fang, and X. Jia, "A compact dual-band and dual-polarized antenna integrated into textile for WBAN dual-mode applications," *Prog. Electromagn. Res. Lett.*, vol. 91, pp. 153–161, 2020, doi: 10.2528/PIERL20032901.
[46] H. A. Mashaghba, H. A. Rahim, P. J. Soh, M. Abdulmalek, I. Adam, M. Jusoh, T. Sabapathy, M. N. M. Yasin, and K. N. A. Rani, "Bending assessment of dual-band split ring-shaped and bar slotted all-textile antenna for off-body WBAN/WLAN and 5G applications," in *Proc. 2nd Int. Conf. Broadband Commun., Wireless Sensors Powering (BCWSP)*, Sep. 2020, pp. 1–5, doi: 10.1109/BCWSP50066.2020.9249403.
[47] H. K. Raad, H. M. Al-Rizzo, A. I. Abbosh, and A. I. Hammoodi, "A compact dual band polyimide based antenna for wearable and flexible telemedicine devices," *Prog. Electromagn. Res. C*, vol. 63, pp. 153–161, 2016, doi: 10.2528/PIERC16010707.

UMAR MUSA (Student Member, IEEE) received the bachelor's degree in electrical engineering from Bayero University Kano, Nigeria, in 2012, and the M.Eng. degree in electronic and telecommunication engineering from Universiti Teknologi Malaysia (UTM), Malaysia, in 2016. He is currently pursuing the Ph.D. degree with the Department of Communication Engineering, Faculty of Electrical and Electronic Engineering, Universiti Tun Hussein Onn Malaysia (UTHM). He is currently a Lecturer with the Department of Electrical Engineering, Bayero University Kano. His research interests include, but are not limited to, the design of RF and microwave devices and active antennas measurement. He is a member of the Council for the Regulation of Engineering of Nigeria, since 2019.

SHAHARIL MOHD SHAH received the B.Eng. degree in microwave and communication from Multimedia University (MMU), in 2002, the M.Sc. degree in microwave engineering and wireless subsystems design from the University of Surrey, U.K., in 2004, and the Ph.D. degree in communication engineering from the University of Birmingham, U.K., in 2016. He is currently a Senior Lecturer with the Department of Communication Engineering, Faculty of Electrical and Electronic Engineering, Universiti Tun Hussein Onn Malaysia (UTHM). His research interests include, but are not limited to, the design of microwave devices, active antennas measurement, and nonlinear characterization of active devices.

HUDA A. MAJID (Member, IEEE) received the B.Eng. degree in electrical engineering (telecommunication) from Universiti Teknologi Malaysia, in 2007, and the M.Eng. and Ph.D. degrees in electrical engineering from Universiti Teknologi Malaysia, in 2010 and 2013, respectively. He is currently a Lecturer with the Department of Electrical Engineering Technology, Faculty of Engineering Technology, Universiti Tun Hussein Onn Malaysia. He has published over 90 articles in journals and conference papers. His research interests include the areas of design of microstrip antennas, small antennas, reconfigurable antennas, metamaterial structure, metamaterial antennas, and millimeter-wave antennas.

ISMAIL AHMAD MAHADI (Student Member, IEEE) received the bachelor's degree in electrical engineering from the Universiti Tun Hussein Onn Malaysia (UTHM), in 2020, where he is currently pursuing the master's degree with the Department of Communication Engineering, Faculty of Electrical and Electronic Engineering. His research interests include wireless power transfer and control systems for AC high-frequency inverters.

MOHAMAD KAMAL A. RAHIM (Senior Member, IEEE) received the B.Eng. degree in electrical and electronic engineering from the University of Strathclyde, U.K., in 1987, the M.Eng. degree in science from the University of New South Wales Australia, in 1992, and the Ph.D. degree in electrical engineering from the University of Birmingham, U.K., in 2003. From 1987 to 1989, he worked as a Management Trainee with Sime Tyres Mer Gong Alor Star Kedah and as a Production Supervisor with Sime Shoes, Kulim, Kedah. He joined the Department of Communication Engineering, Faculty of Electrical Engineering, Universiti Teknologi Malaysia, Kuala Lumpur, as an Assistant Lecturer, in 1989. After receiving his master's, he was appointed as a Lecturer with the Faculty of Electrical Engineering. He was appointed as a Senior Lecturer, in 2005. He was appointed as an Associate Professor with the Faculty. He is currently a Professor of RF and antenna with the Faculty of Electrical Engineering, Universiti Teknologi Malaysia. His research interests include the design of dielectric resonator antennas, microstrip antennas, small antennas, microwave sensors, RFID antennas for readers and tags, multifunction antennas, microwave circuits, EBG, artificial magnetic conductors, metamaterials, phased array antennas, computer-aided design for antennas, and design of millimeter frequency antennas.

MUHAMMAD SANI YAHYA (Graduate Student Member, IEEE) received the B.Eng. degree in electrical and electronics engineering from Abubakar Tafawa Balewa University Bauchi (ATBU), Nigeria, in 2010, and the M.Eng. degree in electronic and telecommunication engineering from Universiti Teknologi Malaysia (UTM), in 2016. He is currently pursuing the Ph.D. degree with the Department of Electrical and Electronics Engineering, Universiti Teknologi Petronas (UTP), Malaysia. He is currently a Lecturer with Abubakar Tafawa Balewa University Bauchi. He has published some papers in both local and international journals and has attended several local and international conferences. His research interests include the area of RF and microwaves: antenna design and characterizations.

ZUHAIRIAH ZAINAL ABIDIN (Senior Member, IEEE) received the Ph.D. degree from Bradford University, U.K., in 2011. She is currently an Associate Professor and the Head of the Advanced Telecommunication Research Center (ATRC), Universiti Tun Hussein Onn Malaysia. She has authored and coauthored several journals and proceedings. Her research interests include MIMO antenna, printed microstrip antenna, wearable antennas, metamaterial resonator, electromagnetic bandgap (EBG) for wireless and mobile, and high-speed digital circuit applications.